Upper-Bounding the Capacity of Optical IM/DD Channels With Multiple-Subcarrier Modulation and Fixed Bias Using Trigonometric Moment Space Method

Roy You, *Student Member, IEEE,* and Joseph M. Kahn, *Fellow, IEEE*

***Abstract*—We consider the channel capacity of an optical intensity-modulated direct-detection (IM/DD) system using multiple-subcarrier modulation (MSM) with fixed bias. The channel is modeled as an additive white Gaussian noise (AWGN) channel with nonnegative input waveform. The mean of the nonnegative input waveform is the average transmitted optical power. The mean of the waveform during a symbol period is called the d.c. bias of the symbol. In this work, a fixed bias is used for all symbols. Therefore, the power used for each symbol is constant and equals the average transmitted power. The main result of this correspondence shows that, because the input waveforms during each symbol period are nonnegative and have fixed mean, their Fourier coefficients must lie inside certain trigonometric moment spaces. These moment spaces are characterized both algebraically and geometrically. Through the geometrical characterization, we determine the volumes of these moment spaces. The channel capacities of quadrature amplitude modulation (QAM) and pulse amplitude modulation (PAM) systems are shown to be upper-bounded by sphere-packing Gaussian noise in the respective moment spaces.**

***Index Terms*—Multiple-subcarrier modulation (MSM), optical intensity-modulated direct-detection (IM/DD) channel, trigonometric moment space.**

I. Introduction

In this correspondence, we are concerned with the channel capacity of an optical intensity-modulated direct-detection (IM/DD) channel. Intensity modulation means that information is modulated onto the intensity of optical signal, which is proportional to the signal's instantaneous power. Direct detection means that the receiver detects the instantaneous power of the received signal. This type of system has been widely used in both fiber and free-space optical communication systems.

Specifically, we study optical multiple-subcarrier modulation systems, where input data is modulated onto orthogonal frequency carriers. In some respect, optical multiple-subcarrier modulation (MSM) systems are very similar to electrical MSM systems, which have been well studied especially because of the popularity of modulation schemes such as discrete multitone modulation (DMT) and orthogonal frequency division multiplexing (OFDM).[1] However, optical MSM signal is different from electrical MSM signal in one key respect. Since the optical MSM signal is modulated onto optical intensity (instantaneous power), the transmitted waveform must be nonnegative, and the average transmitted power is the mean of the input waveform instead of its mean square. In this correspondence, we investigate the consequences of the nonnegativity of input waveform through the properties of its Fourier coefficients while assuming that the input waveform has the same average power during each symbol interval. We explore the facts that the Fourier coefficients of band-limited nonnegative functions must form finite positive semidefinite (p.s.d.) sequences and the convex hull of these finite sequences is bounded by the moment space of trigonometric functions. Therefore, the study of trigonometric moment spaces allows us to determine the regions where the input signals lie, which leads to upper bounds of the channel capacities for optical IM/DD channels. This bounding technique gives us geometrical intuition regarding to the signal space and becomes asymptotically exact for QAM systems.

In summary, we present the following facts in this correspondence.

- The synchronous waveform channel with the band-limited input waveform $x_i(t)$ during its ith symbol interval is equivalent to a discrete-time vector channel with the vector input $[c_{i,n}]_{n=1}^{k}$ for the ith symbol, where the vector $[c_{i,n}]_{n=1}^{k}$ is the set of Fourier series coefficients of the waveform $x_i(t)$. Because the optical IM/DD channel under consideration is memoryless and the noise is white, the channel capacity can be achieved by waveform inputs which are independent and identically distributed (i.i.d.) from symbol to symbol. Thus, the single-shot vector channel model is used in this correspondence.
- For both PAM and QAM systems, during each symbol interval, because of the nonnegativity constraint on the band-limited input waveform $x(t)$, the corresponding vector input $[c_n]_{n=1}^{k}$ must lie inside certain corresponding trigonometric moment spaces.
- The trigonometric moment spaces are first characterized algebraically through p.s.d. sequences. This characterization gives a simple test to see if a sequence is inside a trigonometric moment space.
- Then, the trigonometric moment spaces are characterized geometrically by showing that they are equivalent to the convex hulls of certain curves. The volumes of the moment spaces are calculated subsequently.
- The high-SNR channel capacities of optical IM/DD MSM channels are upper-bounded by sphere-packing Gaussian noise in the moment spaces.
- Further interpretations are given to illuminate the obtained results.

II. Channel Model and Notation

The optical IM/DD channel is often modeled as a baseband linear system [2]

$$Y(t) = R \cdot X(t) \otimes h(t) + N(t) \tag{1}$$

where $Y(t)$ is the output current, R is the photon-detector responsivity, $X(t)$ is the instantaneous input power, $h(t)$ is channel impulse response, $N(t)$ is the channel noise, and $\otimes$ denotes the convolution operation. In this correspondence, we assume that the channel is frequency nonselective (i.e., $h(t) = H \cdot \delta(t)$) and the noise $N(t)$ is white and Gaussian with power spectral density[2] N_0. These are appropriate assumptions for optical systems dominated by thermal electrical noise and/or strong ambient light noise (such as line-of-sight free-space optical systems and fiber-optical systems with negligible dispersion) [3]. With the above assumptions, we will simply rewrite the channel model as

$$Y(t) = R \cdot H \cdot X(t) + N(t). \tag{2}$$

Manuscript received November 6, 2000; revised June 6, 2001. This work was supported by the National Science Foundation under Grant ECS-9710065. The material in this correspondence was presented in part at the International Conference on Communications, Helsinki, Finland, 2001.

The authors are with the Department of Electrical Engineering and Computer Sciences, University of California, Berkeley CA 94720 USA (e-mail: ryou; @eecs.berkeley.edu; jmk@eecs.berkeley.edu).

Communicated by G. Caire, Associate Editor for Communications.

Publisher Item Identifier S 0018-9448(02)00305-X.

[1]For an introductory exposition of MSM schemes on electrical signals, we refer the reader to [1].

[2]This is to say that $R_N(\tau) = E[N(t+\tau)N^*(t)] = N_0\delta(\tau)$ and $\Phi_N(f) = N_0$.

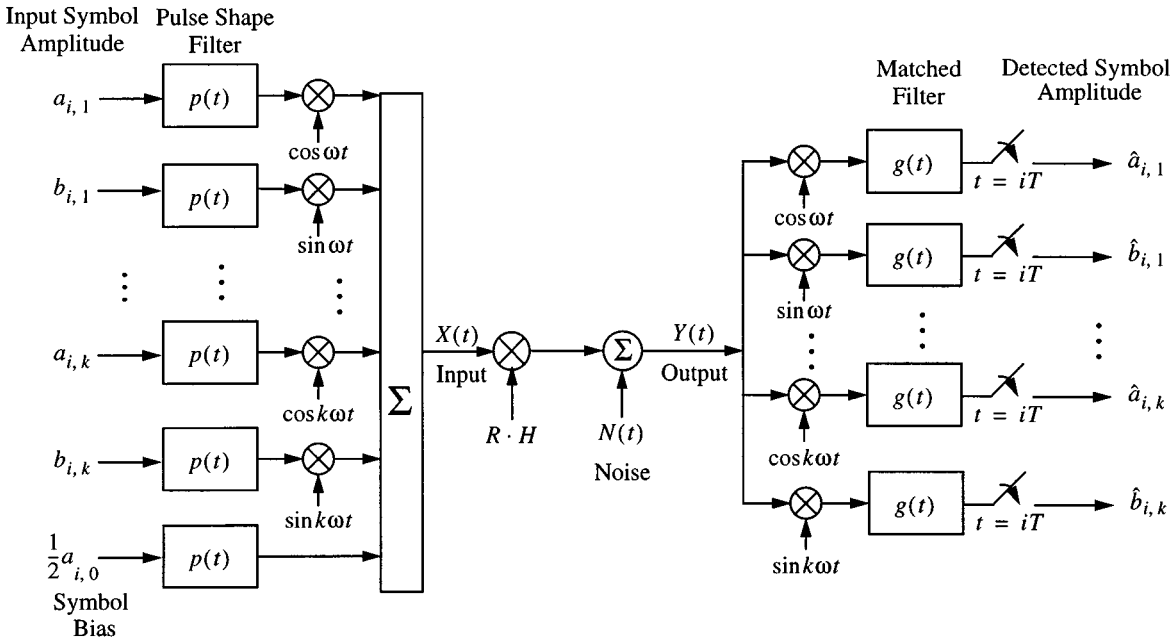

Fig. 1. Channel model.

Furthermore, in this correspondence, we deal with multiple subcarrier systems, where input data is modulated onto orthogonal frequency carriers. The channel model is shown in Fig. 1. The input waveform over all time is

$$X(t) = \sum_{i=-\infty}^{\infty} x_i(t)p(t - iT) \tag{3}$$

where $\frac{\omega}{2\pi}$ is the frequency separation between subcarriers, $T = \frac{2\pi}{\omega}$ is the symbol duration, $p(t)$ is the mean amplitude pulse shape function

$$p(t) = \begin{cases} P, & 0 \le t < T \\ 0, & \text{otherwise} \end{cases} \tag{4}$$

with $P > 0$. $x_i(t)$ is a real nonnegative input waveform for the ith signaling interval. Because we use multiple subcarrier modulation, $x_i(t)$ is of the following form:

$$\begin{aligned} x_i(t) &= \sum_{n=-k}^{k} c_{i,n}\, e^{-jn\omega t} \\ &= \frac{1}{2}\, a_{i,0} + \sum_{n=1}^{k} a_{i,n} \cos(n\omega t) + \sum_{n=1}^{k} b_{i,n} \sin(n\omega t) \end{aligned} \tag{5}$$

where

$$[c_{i,n}]_{n=1}^{k} \triangleq [c_{i,-n}^{*}]_{n=1}^{k} \triangleq \left[\frac{1}{2}(a_{i,n} + jb_{i,n})\right]_{n=1}^{k}$$

denotes the information transmitted during the ith symbol interval. $c_{i,-n}^{*}$ denotes the complex conjugate of $c_{i,-n}$, and k is the number of subcarriers excluding baseband.

Because of the conjugate symmetry, the term $c_{i,0} = \frac{1}{2}\, a_{i,0}$ is always real. Furthermore, for nonnegative $x_i(t)$, $c_{i,0}$ must be nonnegative and does not equal zero unless all other terms vanish [4]. Thus, we call $\frac{1}{2}\, a_{i,0}P$ the d.c. bias, since it ensures the nonnegativity of input waveform $X(t)$. It has been shown that in binary phase shift keying (BPSK) and quadrature phase shift keying (QPSK) optical MSM systems, average-power efficiency can be improved if the bias ($\frac{1}{2}\, a_{i,0}P$) is allowed to vary from symbol to symbol [5]. However, most optical MSM systems use a fixed bias for the simplicity of implementation. Therefore, we consider the fixed bias case and let $\frac{1}{2}\, a_{i,0}P$ be a constant. Without loss of generality, we can allow P to take care of the mean amplitude scaling and let $\frac{1}{2}\, a_{i,0} = 1$. Since $\frac{1}{2}\, a_{i,0} = 1$ for each symbol, there is no information conveyed through the bias. Hence, for PAM, using k carriers is equivalent to having k orthogonal channels; for QAM, using k carriers is equivalent to having $2k$ orthogonal channels. Because $p(t)$ is a rectangular pulse of duration T, the power spectrum of each modulated subcarrier has nulls at frequency $\pm\frac{1}{T}$ hertz above and below the subcarrier frequency. The total bandwidth required by the k-subcarrier signal $X(t)$ is therefore considered to be

$$W = \frac{k+1}{T} \tag{6}$$

hertz, which corresponds to the first null in the power spectrum of $X(t)$ above the highest subcarrier frequency.

To recover information, the received waveform $Y(t)$ is passed through a matched-filter demodulator where $g(t)$ is matched to $p(t)$ and is normalized to have an energy of 2. Hence,

$$g(t) = \begin{cases} \sqrt{\frac{2}{T}}, & 0 \le t < T \\ 0, & \text{otherwise.} \end{cases} \tag{7}$$

Thus, the output of the demodulator will be

$$\hat{a}_{i,n} = \int_0^T Y(t)g(t)\cos(n\omega t)\, dt = RHP\sqrt{\frac{T}{2}}\, a_{i,n} + n_{i,n}^{c} \tag{8}$$

$$\hat{b}_{i,n} = \int_0^T Y(t)g(t)\sin(n\omega t)\, dt = RHP\sqrt{\frac{T}{2}}\, b_{i,n} + n_{i,n}^{s} \tag{9}$$

where $n_{i,n}^{c}$ and $n_{i,n}^{s}$ are independent and of $\mathcal{N}(0, N_0)$ distributions.

For compactness of notation, we denote

$$c_{i,n} = \frac{1}{2}(a_{i,n} + jb_{i,n}) \tag{10}$$

$$n_{i,n} = \frac{1}{2}(n_{i,n}^{c} + jn_{i,n}^{s}) \tag{11}$$

$$\hat{c}_{i,n} = \frac{1}{2}(\hat{a}_{i,n} + j\hat{b}_{i,n}). \tag{12}$$

Then, after the above manipulation, the waveform channel is represented equivalently by the vector channel

$$[\hat{c}_{i,n}]_{n=1}^{k} = RHP\sqrt{\frac{T}{2}}\,[c_{i,n}]_{n=1}^{k} + [n_{i,n}]_{n=1}^{k}, \qquad i \in \mathbb{Z} \tag{13}$$

with the further requirement that $[c_{i,n}]_{n=1}^{k}$ represents nonnegative $x_i(t)$. Notice that, for PAM systems, the imaginary part of the above equation will be discarded and $n_{i,n}$'s are i.i.d. real Gaussian random

variables with variance $\frac{N_0}{4}$, while for QAM, $b_{i,n} \not\equiv 0$ and $n_{i,n}$'s are i.i.d. proper complex Gaussian random variables with variance $\frac{N_0}{2}$.

Since the channel is memoryless and the noise is i.i.d. from symbol to symbol, the channel capacity can be achieved by i.i.d. vector inputs. Therefore, to calculate the channel capacity, we only need to consider the capacity of one signaling interval. Thus, we will consider this single-shot vector channel model in the remainder of the correspondence. From now on, we will drop the subscript i for the ith symbol and denote our input waveform during the considered symbol duration as $x(t)$.

III. Input Constraints and Relaxation

The most important difference between an optical IM/DD channel and a conventional electrical channel is that the optical channel input is intensity. This has two significant consequences. First, since the input is intensity, it must be nonnegative. Second, since the input is intensity, the average optical power is proportional to the mean of the input. Therefore, we impose these two constraints on the optical IM/DD channel input

$$x(t)p(t) \geq 0, \qquad t \in [0, T) \tag{14}$$

$$P_{\text{av}} = E\left[\frac{1}{T}\int_0^T x(t)p(t)\,dt\right] = E\left[\frac{1}{2}\,a_0 P\right]. \tag{15}$$

However, in previous section, we have reformulated the optical IM/DD channel model from a waveform channel with input $x(t)$ to a vector channel with input $[c_n]_{n=1}^k$. Thus, we need to impose the constraints on the vector input correspondingly.

The power constraint can be easily satisfied. Since we use fixed bias for each symbol, $\frac{1}{2}\,a_0 P$ is a constant and equals average power P_{av}. Because $\frac{1}{2}\,a_0 = 1$, we see that the average transmitted optical power equals P

$$P_{\text{av}} = P. \tag{16}$$

Furthermore, we still need to impose the nonnegativity constraint onto the corresponding vector representation $[c_n]_{n=1}^k$. We define the sets of Fourier coefficient sequences representing band-limited nonnegative functions for PAM and QAM systems as

$$\mathcal{CH}_k^P = \left\{[c_n]_{n=1}^k \colon 1 + \sum_{n=1}^k a_n \cos(n\omega t) \geq 0, c_n = \frac{1}{2}\,a_n\right\} \tag{17}$$

$$\mathcal{CH}_k^Q = \left\{[c_n]_{n=1}^k \colon 1 + \sum_{n=1}^k a_n \cos(n\omega t) + b_n \sin(n\omega t) \geq 0, \quad c_n = \frac{1}{2}\,(a_n + jb_n)\right\}. \tag{18}$$

It is desired to find the necessary and sufficient conditions on the sequence $[c_n]_{n=1}^k$ such that it represents a nonnegative trigonometric polynomial $x(t)$ for PAM and QAM, correspondingly. Unfortunately, we cannot find such conditions because of the band-limited nature of $x(t)$.

However, if we relax the band-limit condition on $x(t)$, the problem of nonnegativity can be easily solved. For PAM, the sequence $[c_n]_{n=1}^k$ must fall in the finite-dimensional cosine moment space

$$\mathcal{M}_k^P = \left\{[c_n']_{n=1}^k \colon c_n' = \frac{1}{T}\int_0^T \cos(n\omega t)x'(t)\,dt,\ x'(t) \geq 0, \quad \frac{1}{T}\int_0^T x'(t)\,dt = 1\right\}. \tag{19}$$

For QAM, the sequence $[c_n]_{n=1}^k$ must fall in the finite-dimensional trigonometric moment space

$$\mathcal{M}_k^Q = \left\{[c_n']_{n=1}^k \colon c_n' = \frac{1}{T}\int_0^T e^{jn\omega t}x'(t)\,dt,\ x'(t) \geq 0, \quad \frac{1}{T}\int_0^T x'(t)\,dt = 1\right\}. \tag{20}$$

It is obvious that $\mathcal{CH}_k^P$ and $\mathcal{CH}_k^Q$ lie inside $\mathcal{M}_k^P$ and $\mathcal{M}_k^Q$, respectively, which gives the condition necessary for $[c_n]_{n=1}^k$ to represent a nonnegative input waveform $x(t) \geq 0$, $t \in [0, T)$ for PAM and QAM systems. However, we emphasize that these conditions are only necessary but not sufficient. Although it is true that each point inside $\mathcal{M}_k^P$ and $\mathcal{M}_k^Q$ has at least one corresponding (not necessarily band-limited) nonnegative function $x'(t)$, it is not true that each point can represent a band-limited nonnegative function $x(t)$ with k subcarriers, because in the definition of moment spaces $x'(t)$ is not necessarily band-limited as we have imposed upon our intensity input function $x(t)$.

Thus, for a general $x'(t)$, it may be necessary to use an infinite sequence $[c_n']_{n=1}^\infty$ to specify it, where $[c_n']_{n=1}^k$ is only the truncation of the infinite sequence in the first k terms. However, the trigonometric moment spaces $\mathcal{M}_k^P$ and $\mathcal{M}_k^Q$ do provide upper bounds to the sets of possible input $\mathcal{CH}_k^Q$ and $\mathcal{CH}_k^P$. Furthermore, in the case of QAM, because the input function $x(t)$ is specified by the set of basis functions $\{\cos(n\omega t), \sin(n\omega t),\ n = 1, 2, \ldots, k\}$, then, as the number of subcarriers k grows large, the set $\mathcal{CH}_k^Q$ approaches the set of arbitrary nonnegative input waveforms, which is also the limit of the trigonometric moment space $\mathcal{M}_k^Q$. Thus, we can consider the bound for QAM systems becomes asymptotically exact as k goes to infinity.

As we can see, the problem of communicating over optical IM/DD MSM channels is intimately related with the characterization of trigonometric moment spaces. The definitions of trigonometric moment spaces $\mathcal{M}_k^P$ and $\mathcal{M}_k^Q$ given so far are only conceptual. We need some operational definitions of the moment spaces to tell us more about where the sequences $[c_n']_{n=1}^k$ lie. We do this in the next section.

IV. Trigonometric Moment Spaces

In this section, we will characterize the trigonometric moment spaces both algebraically and geometrically. The algebraic characterization is through p.s.d. sequences, while the geometric characterization is through convex hulls of certain curves. Although the geometric characterization is more direct and provides more insight for the capacity bounding problem, the algebraic characterization gives us an easy test to see if a sequence lies inside the trigonometric moment spaces. Thus, we will present both characterizations subsequently.

A. Algebraic Characterization

First, we consider the case of complex $[c_n']_{n=1}^k$, which corresponds to $\mathcal{M}_k^Q$. A sequence $[c_n']_{n=1}^k$ of complex numbers is called *positive semidefinite* if and only if

$$\sum_{i=1}^n \sum_{j=1}^n \rho_i^* c_{i-j}' \rho_j \geq 0, \qquad \text{where } c_{-n}' \triangleq c_n'^*,\ c_0' \triangleq 1 \tag{21}$$

for all sets of complex numbers $\{\rho_1, , \ldots, \rho_n\}$ where $1 \leq n \leq k$ [4]. In [4], it is also shown that $[c_n']_{n=1}^k$ is p.s.d. if and only if there is a function $x'(t) \geq 0$ such that

$$c_n' = \frac{1}{T}\int_0^T e^{jn\omega t}x'(t)\,dt, \qquad \text{where } T = \frac{2\pi}{\omega}. \tag{22}$$

Therefore, $[c_n']_{n=1}^k \in \mathcal{M}_k^Q$ is equivalent to requiring that the complex sequence $[c_n']_{n=1}^k$ forms a p.s.d. sequence. Conversely, $[c_n']_{n=1}^k$ being p.s.d. implies that $[c_n']_{n=1}^k \in \mathcal{M}_k^Q$. Furthermore, it has been shown [6] that a sequence $[c_n']_{n=1}^k$ is p.s.d. if and only if its Toeplitz matrix C_n'

is a p.s.d. matrix for all $0 \le n \le k$, where the Toeplitz matrix of the sequence $[c_n']_{n=1}^k$ is defined as follows for $0 \le n \le k$:

$$C_n' = \begin{bmatrix} c_0' & c_1' & \cdots & c_n' \\ c_{-1}' & c_0' & \cdots & c_{n-1}' \\ \vdots & \vdots & \ddots & \vdots \\ c_{-n}' & c_{n-1}' & \cdots & c_0' \end{bmatrix}, \; c_{-n}' \triangleq c'^*_n, \; c_0' \triangleq 1$$

$$= \begin{bmatrix} c_0' & c_1' & \cdots & c_n' \\ c'^*_1 & c_0' & \cdots & c_{n-1}' \\ \vdots & \vdots & \ddots & \vdots \\ c'^*_n & c'^*_{n-1} & \cdots & c_0' \end{bmatrix}. \tag{23}$$

This set of necessary and sufficient conditions on $[c_n']_{n=1}^k$ gives the first operational characterization of $\mathcal{M}_k^Q$

$$\mathcal{M}_k^Q = \{[c_n']_{n=1}^k \colon C_n' \text{ is p.s.d. for all } 0 \le n \le k, \; c_n' \text{ is complex}\}. \tag{24}$$

Similarly, we can find the algebraic characterization of $\mathcal{M}_k^P$

$$\mathcal{M}_k^P = \{[c_n']_{n=1}^k \colon C_n' \text{ is p.s.d. for all } 0 \le n \le k, \; c_n' \text{ is real}\}. \tag{25}$$

Although it is possible to use the p.s.d. property to characterize $\mathcal{M}_k^Q$ and $\mathcal{M}_k^P$ [7], it is much easier to check the positive definiteness of C_n', which defines the interior regions of the moment spaces. To find the interior regions of the moment spaces, we can use the leading principal minor test

$$\begin{aligned} \det C_0' &= \det\left[c_0'\right] > 0 \\ \det C_1' &= \det\begin{bmatrix} c_0' & c_1' \\ c'^*_1 & c_0' \end{bmatrix} > 0 \\ \det C_2' &= \det\begin{bmatrix} c_0' & c_1' & c_2' \\ c'^*_1 & c_0' & c_1' \\ c'^*_2 & c'^*_1 & c_0' \end{bmatrix} > 0 \\ &\vdots \end{aligned} \tag{26}$$

Given $c_0' \triangleq 1$, we carry out the calculation of the above conditions and obtain the following:

$$\begin{aligned} 1 &> 0 \\ 1 - \|c_1'\|^2 &> 0 \\ 1 - 2\|c_1'\|^2 - \|c_2'\|^2 + c_1' c_1' c'^*_2 + c'^*_1 c'^*_1 c_2' &> 0 \\ &\vdots \end{aligned} \tag{27}$$

The interior region of $\mathcal{M}_k^Q$ is defined by the set of complex sequences $[c_n']_{n=1}^k$ that satisfies all the constraints above, while the interior region of $\mathcal{M}_k^P$ is defined by the set of real sequence satisfying the conditions. The boundaries of the moment spaces can be approached arbitrarily close by the interior points and have measure 0.

However, as we can see, this algebraic characterization becomes complicated as the number of subcarriers k increases. It requires a different approach to characterize the trigonometric moment spaces.

B. Geometric Characterization

In this subsection, we characterize the trigonometric moment spaces $\mathcal{M}_k^P$ and $\mathcal{M}_k^Q$ from a geometrical approach. For this purpose, we first define two space curves

$$\mathcal{E} = \{[V_n(t)]_{n=1}^k \colon [V_n(t)]_{n=1}^k = [e^{j\omega t} e^{j2\omega t} \cdots e^{jk\omega t}]^T, \; t \in [0, T)\} \tag{28}$$

$$\mathcal{C} = \{[v_n(t)]_{n=1}^k \colon [v_n(t)]_{n=1}^k = [\cos(\omega t) \; \cos(2\omega t) \cdots \cos(k\omega t)]^T, \; t \in [0, T)\}. \tag{29}$$

The key fact presented here is that the trigonometric moment spaces are equivalent to the convex hulls of these space curves and the volume of the convex hulls can be determined.

The convex hull of a set is defined as the smallest convex set containing the original set [8]. We denote the convex hull of $\mathcal{E}$ and $\mathcal{C}$ as $\mathrm{conv}(\mathcal{E})$ and $\mathrm{conv}(\mathcal{C})$, correspondingly. We want to show that $\mathcal{M}_k^Q = \mathrm{conv}(\mathcal{E})$ and $\mathcal{M}_k^P = \mathrm{conv}(\mathcal{C})$.

Here, we first derive the complex case which corresponds to $\mathcal{M}_k^Q$. Given the conceptual definition of $\mathcal{M}_k^Q$, we realize that we can define the vector $[c_n']_{n=1}^k \in \mathcal{M}_k^Q$ as

$$[c_n']_{n=1}^k = \frac{1}{T}\int_0^T x'(t)[V_n(t)]_{n=1}^k \, dt, \qquad \text{where } [V_n(t)]_{n=1}^k \in \mathcal{E}. \tag{30}$$

If we consider the curve $\mathcal{E}$ as a set of points, then, because $x'(t) \ge 0$ and $\frac{1}{T}\int_0^T x'(t)\,dt = 1$, we can see that $[c_n']_{n=1}^k$ is actually the convex combination of the points $[V_n(t)]_{n=1}^k$ in $\mathcal{E}$ with $x'(t)$ as the weight for each point. Thus, $\mathcal{M}_k^Q \subseteq \mathrm{conv}(\mathcal{E})$.

To show that $\mathrm{conv}(\mathcal{E}) \subseteq \mathcal{M}_k^Q$, we use the separating hyperplane theorem [8]. Suppose there exists a point $[c_n']_{n=1}^k \in \mathcal{M}_k^Q$ that does not belong to $\mathrm{conv}(\mathcal{E})$. Then, by the separating hyperplane theorem, there exists a vector $[\lambda_n]_{n=1}^k \not\equiv 0$ and a real constant μ such that

$$\Re\left[\sum_{n=1}^k \lambda_n^* c_n'\right] < \mu \tag{31}$$

$$\Re\left[\sum_{n=1}^k \lambda_n^* V_n\right] \ge \mu, \qquad \forall [V_n]_{n=1}^k \in \mathrm{conv}(\mathcal{E}). \tag{32}$$

Then, for all $[V_n(t)]_{n=1}^k \in \mathcal{E}$, we have

$$\Re\left[\sum_{n=1}^k \lambda_n^* V_n(t)\right] \ge \mu.$$

Thus,

$$\Re\left[\frac{1}{T}\int_0^T x'(t)\left[\sum_{n=1}^k \lambda_n^* V_n(t)\right] dt\right] = \Re\left[\sum_{n=1}^k \lambda_n^* c_n'\right] \ge \mu. \tag{33}$$

We have reached a contradiction. Therefore, $\mathrm{conv}(\mathcal{E}) \subseteq \mathcal{M}_k^Q$. Consequently, $\mathcal{M}_k^Q = \mathrm{conv}(\mathcal{E})$.

Similarly, we can show that $\mathrm{conv}(\mathcal{C}) = \mathcal{M}_k^P$. The two- and three-dimensional examples of $\mathcal{M}_k^P$ are shown in Fig. 2.

More importantly, the geometrical characterization gives us information regarding to the volume of the trigonometric moment spaces.

We have shown that $\mathcal{M}_k^Q = \mathrm{conv}(\mathcal{E})$. As we recognize, the curve $\mathcal{E}$ is a linear transformation of the generalized ellipse

$$\mathcal{GE} = \left\{\left[\frac{1}{n}(\cos n\omega t + j \sin n\omega t)\right]_{n=1}^k : t \in \left[0, \frac{2\pi}{\omega}\right)\right\}.$$

It has been shown [9] that the volume of $\mathrm{conv}(\mathcal{GE})$ is

$$V = \frac{2^k \pi^k}{k!(2k)!}. \tag{34}$$

Applying the linear transformation to $\mathcal{E}$, we get the volume of $\mathcal{M}_k^Q$

$$V_k^Q = (k!)(k!) \cdot V = \frac{2^k \pi^k k!}{(2k)!}. \tag{35}$$

For $\mathcal{M}_k^P$, the analytical expression for the volume of the $\mathrm{conv}(\mathcal{C})$ is given in [10]

$$V_k^P = 2^k \prod_{i=1}^k \left(\frac{2i}{2i+1}\right)^{k-i}, \qquad k > 0 \tag{36}$$

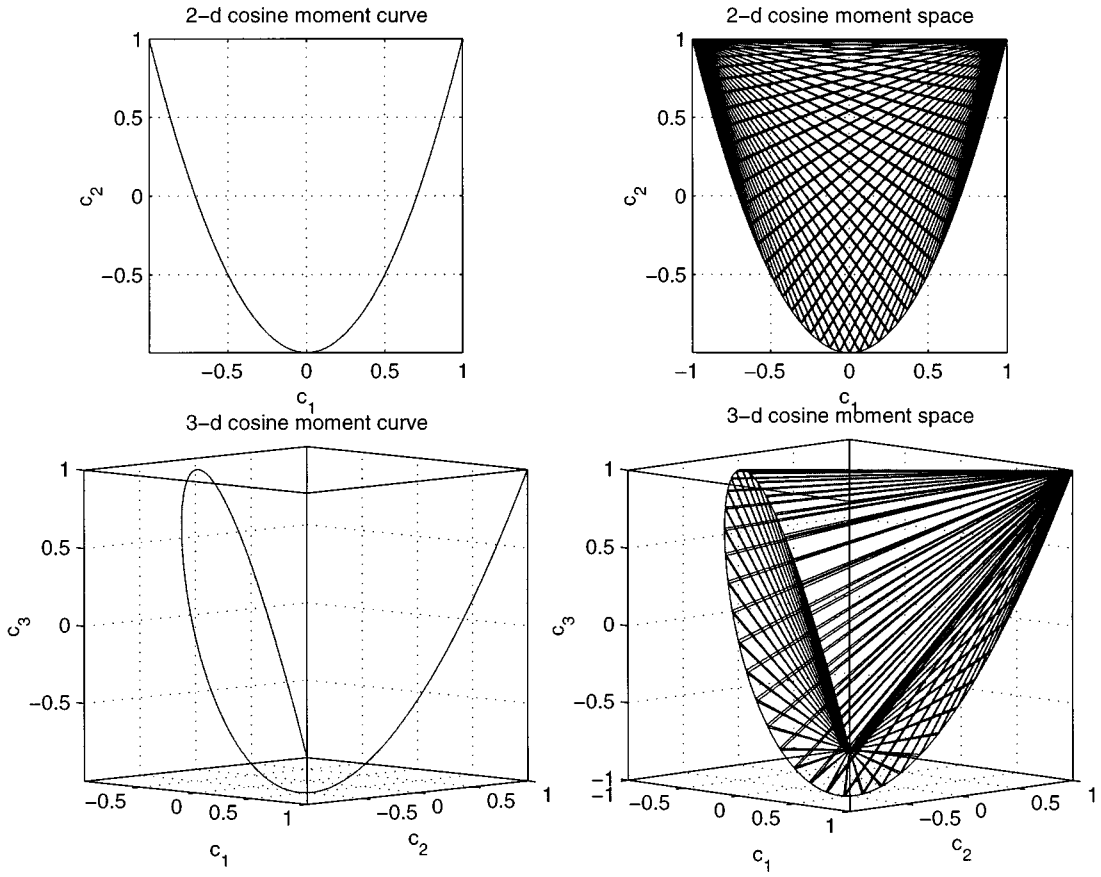

Fig. 2. Examples of cosine moment spaces.

where the above simple result is derived by observing certain relationship between the autocorrelation sequence (p.s.d) and the reflection coefficients. However, we remark that it can also be derived by a linear transformation of the polynomial moment space. It has been shown [11] that for $\{[t^n]_{n=1}^k\colon t \in [0, 1]\}$, the volume of the convex hull of this moment curve is

$$V' = \prod_{i=1}^{k} \frac{\Gamma(i)\Gamma(i)}{\Gamma(2i)}, \qquad \text{where } \Gamma(i) \text{ is the gamma function.} \tag{37}$$

Then, let

$$\begin{aligned} \cos\theta &= x & x &= (2t-1) \\ \cos 2\theta &= 2x^2 - 1 & x^2 &= (2t-1)^2 \\ \cos 3\theta &= 4x^3 - 3x & x^3 &= (2t-1)^3 \\ &\vdots & &\vdots \end{aligned} \tag{38}$$

Note that the first column is a set of Chebyshev polynomials of the first kind, while the second column is simply a substitution of a variable. It is obvious that there is a linear transformation from $[t^n]_{n=1}^k$ to $[\cos n\theta]_{n=1}^k$. Since the two transformations are both triangular, it is easy to find the Jacobian, and we find that $J = 2^{k^2}$. Then, we have

$$V_k^P = J \cdot V' = 2^{k^2} \cdot V'. \tag{39}$$

Now, for both $\mathcal{M}_k^P$ and $\mathcal{M}_k^Q$, we have characterized the trigonometric moment spaces geometrically as convex hulls of certain curves. This characterization not only tells us where the input sequences must lie but also gives us the volume of the trigonometeric moment spaces. Knowing the volume of the moment spaces, we can derive the upper bounds to the optical IM/DD MSM channel capacities using the argument of sphere-packing Gaussian noise in the moment spaces.

V. Channel Capacity Bounds

In this section, we derive the optical IM/DD channel capacity bounds using the sphere-packing argument. Because there is a clear parallel existing between the PAM case and the QAM case, we will primarily derive our result for PAM and state the result for QAM later.

Through the demodulation process, we get

$$\begin{aligned} [\hat{a}_n]_{n=1}^k &= \int_0^T [RHPx(t) + N(t)] \\ &\quad \cdot \sqrt{\frac{2}{T}} [\cos\omega t \ \cos 2\omega t \ \cdots \ \cos n\omega t]^T \, dt \\ &= RHP\sqrt{\frac{T}{2}}\,[a_n]_{n=1}^k + [n_n^c]_{n=1}^k. \end{aligned} \tag{40}$$

To simplify the vector notations, we define $\boldsymbol{Y} = \frac{1}{2}[\hat{a}_n]_{n=1}^k$, $\boldsymbol{X} = \frac{1}{2}[a_n]_{n=1}^k$, and $\boldsymbol{N} = \frac{1}{2}[n_n^c]_{n=1}^k$. Then, for PAM

$$\boldsymbol{Y} = RHP\sqrt{\frac{T}{2}}\,\boldsymbol{X} + \boldsymbol{N} \tag{41}$$

where $\boldsymbol{Y}$ and $\boldsymbol{X}$ are real vectors and $\boldsymbol{N} \sim \mathcal{N}(0, \frac{N_0}{4} I_k)$. We define the SNR over the bandwidth of one subcarrier as

$$\text{SNR} = \frac{(RHP)^2 T}{N_0} \tag{42}$$

and the normalized noise variance is defined as $\sigma^2 = 1/\text{SNR}$. To simplify the presentation, we further introduce the notations

$$\boldsymbol{Y}' = \boldsymbol{Y} / \left(RHP\sqrt{\frac{T}{2}} \right)$$

and

$$\boldsymbol{N}' = \boldsymbol{N} / \left(RHP\sqrt{\frac{T}{2}} \right).$$

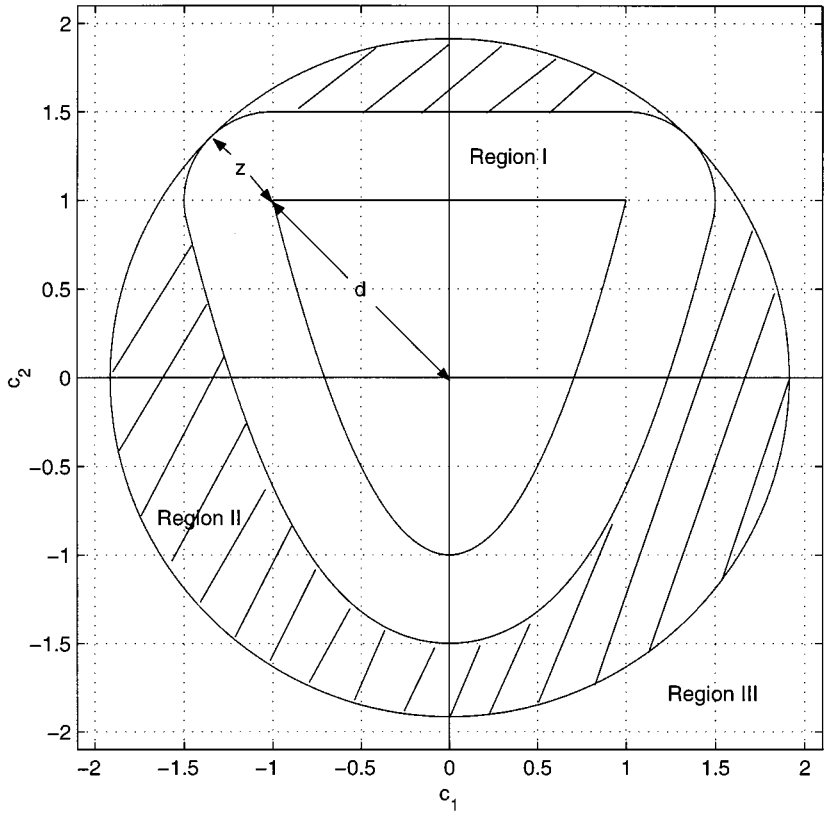

Fig. 3. Three regions of entropy integration.

Then, we have

$$\boldsymbol{Y}' = \boldsymbol{X} + \boldsymbol{N}', \qquad \boldsymbol{N}' \sim \mathcal{N}\left(0, \frac{\sigma^2}{2} I_k\right). \tag{43}$$

The capacity between $\boldsymbol{X}$ and $\boldsymbol{Y}$ is defined as follows, where the supremum is taken over all distributions of $\boldsymbol{X}$ corresponding to nonnegative input waveforms:

$$C_{PAM}^k = \frac{1}{T} \sup_{P_{\boldsymbol{X}}: \boldsymbol{X} \in \mathcal{CH}_k^P} I(\boldsymbol{X}; \boldsymbol{Y}). \tag{44}$$

The mutual information between $\boldsymbol{X}$ and $\boldsymbol{Y}$ is

$$\begin{aligned} I(\boldsymbol{X}; \boldsymbol{Y}) &= h(\boldsymbol{Y}) - h(\boldsymbol{N}) \\ &= h(\boldsymbol{Y}') + k \log\left(RHP\sqrt{\frac{T}{2}}\right) - \frac{k}{2} \log\left(2\pi e \frac{N_0}{4}\right) \\ &= h(\boldsymbol{Y}') + \frac{k}{2} \log \frac{(RHP)^2 T}{\pi e N_0}. \end{aligned} \tag{45}$$

Since the noise $\boldsymbol{N}$ is Gaussian, the output $\boldsymbol{Y}$ is a continuous-valued random vector with a smooth nonzero probability density function everywhere, which means that it has well-defined differential entropy $h(\boldsymbol{Y})$. $\boldsymbol{Y}'$ is only a rescaling of $\boldsymbol{Y}$, hence, the differential entropy $h(\boldsymbol{Y}')$ is also well defined. To find the capacity, we need to maximize $h(\boldsymbol{Y}')$ by varying the input distribution $P_{\boldsymbol{X}}$ with the constraint that $\boldsymbol{X}$ is in the region of possible inputs $\mathcal{CH}_k^P$. However, for an additive white Gaussian noise (AWGN) channel, at high SNR, $\boldsymbol{Y}'$ will almost entirely be bounded within where $\boldsymbol{X}$ is distributed. Thus, the differential entropy $h(\boldsymbol{Y}')$ will mostly consist of the contribution of $\boldsymbol{Y}'$ within the possible input region $\mathcal{CH}_k^P$ with some residue. Because we do not have an operational characterization for $\mathcal{CH}_k^P$, we use the geometrical characterization for $\mathcal{M}_k^P$ as an upper bound. Because the differential entropy function $h(\cdot)$ is concave with respect to smooth distributions over bounded support, the maximum possible entropy contribution of $\boldsymbol{Y}'$ around $\mathcal{M}_k^P$ will be the differential entropy of uniform distribution in $\mathcal{M}_k^P$. Denoting the random vector with the uniform distribution in $\mathcal{M}_k^P$ as $\boldsymbol{X}_{\text{unif}}$, we want to show that

$$h(\boldsymbol{Y}') \le h(\boldsymbol{X}_{\text{unif}}) + o(\sigma) \tag{46}$$

where $o(\sigma)$ is the entropy residue, which vanishes exponentially fast as $\sigma \to 0$.

The detailed proof of the above inequality is shown in the Appendix. However, we give a brief outline here. As we said before, when the SNR is high (i.e., $\sigma \to 0$), $\boldsymbol{Y}'$ is approximately bounded within $\mathcal{M}_k^P$. Thus, the uniform distribution in $\mathcal{M}_k^P$ will bound $h(\boldsymbol{Y}')$. To make this claim concrete, we use the following strategy. We divide the whole $\mathbb{R}^k$ space into three regions as shown in Fig. 3. Region I is the extension of the cosine moment space in all direction by length z, where

$$z = \sqrt{-k\sigma^2 \log 2\pi\sigma^2 - \sigma^2 \log \sigma^2} \tag{47}$$

is a function of the noise variance σ^2 and the system dimension k. Notice that the extension length z will shrink with smaller σ^2. Region II is the gap between the moment space extension and the smallest sphere encircling the moment space extension. This sphere is centered at origin with the radius $d + z$, where

$$d = \sup_{\boldsymbol{x} \in \mathcal{M}_{\boldsymbol{k}}^{\boldsymbol{P}}} \|\boldsymbol{x}\| \tag{48}$$

is the length of the outermost point belonging to the cosine moment space. Region III is the part outside of the sphere. As the SNR becomes high, the entropy of $\boldsymbol{Y}'$, $h(\boldsymbol{Y}')$, vanishes in regions II and III, while region I approaches the cosine moment space. Thus, we claim

$$h(\boldsymbol{Y}') \le h(\boldsymbol{X}_{\text{unif}}) + o(\sigma).$$

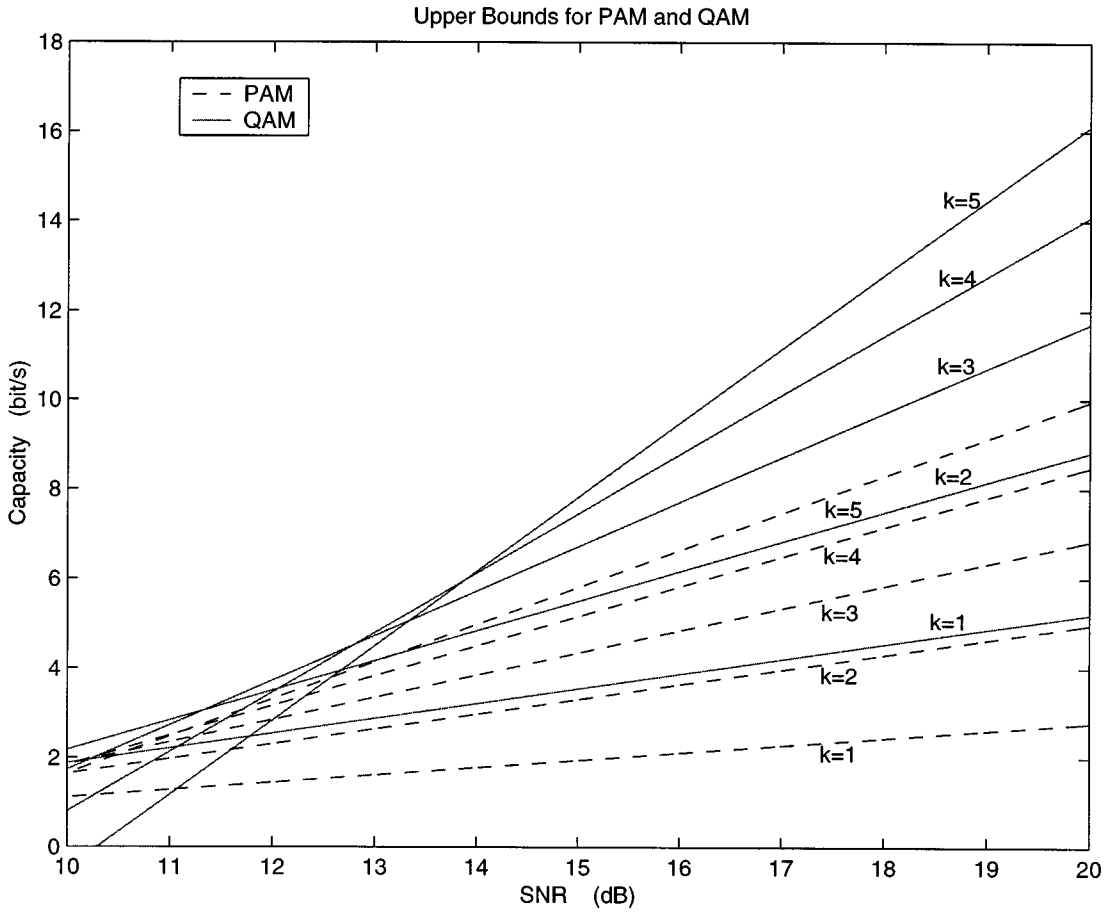

Fig. 4. The capacity bounds of PAM and QAM systems.

The entropy of $\boldsymbol{X}_{\text{unif}}$ is the logarithm of the volume of cosine moment space V_k^P. Then, we get the upper bound to capacity

$$C_{\text{PAM}}^k \leq \frac{1}{T}\left[\log V_k^P + \frac{k}{2}\log\frac{(RHP)^2T}{\pi e N_0} + o(\sigma)\right]. \tag{49}$$

For QAM, a similar argument can be given except that $\boldsymbol{Y}$ and $\boldsymbol{X}$ are complex vectors, $\boldsymbol{N} \sim \mathcal{CN}(0, \frac{N_0}{2} I_k)$, and the possible input and bounding regions are $\mathcal{CH}_k^Q$ and $\mathcal{M}_k^Q$. With these substitutions, we get

$$C_{\text{QAM}}^k \leq \frac{1}{T}\left[\log V_k^Q + k\log\frac{(RHP)^2T}{\pi e N_0} + o(\sigma)\right]. \tag{50}$$

VI. Results and Interpretations

From the previous section, we obtain the following results. For PAM systems, the channel capacity is bounded by

$$C_{\text{PAM}}^k \leq \frac{1}{T}\left(\log\left[2^k\prod_{i=1}^{k}\left(\frac{2i}{2i+1}\right)^{k-i}\right] + \frac{k}{2}\log\left[\frac{(RHP)^2T}{\pi e N_0}\right] + o(\sigma)\right). \tag{51}$$

For QAM systems, the channel capacity is bounded by

$$C_{\text{QAM}}^{2k} \leq \frac{1}{T}\left(\log\left[\frac{2^k\pi^k k!}{(2k)!}\right] + k\log\left[\frac{(RHP)^2T}{\pi e N_0}\right] + o(\sigma)\right). \tag{52}$$

The capacity bounds are shown in Fig. 4 for a different number of subcarriers in PAM and QAM systems, respectively. It is worth noticing that the capacity increment has diminishing return with the number of subcarriers. Because the subcarrier separation is fixed at $\frac{1}{T}$ hertz, using more subcarriers does indeed increase the total system capacity. However, to maintain nonnegativity of input waveform, each subsequently added subcarrier is constrained by the preceding subcarriers. Thus, the capacity increment will not be linear in the number of subcarriers. Therefore, as a result, the spectral efficiency of the multiple subcarrier system suffers. Also, the upper bound of capacity shown in the figure is not the tightest possible, because we made some approximations to achieve the analytical bound. Thus, a more exact upper bound can be obtained if it is calculated numerically.

We now try to analyze the obtained results to obtain further insight. Because of the compactness of the QAM result, we will use it as an example. Using Stirling's formula for the factorial

$$n! \cong \sqrt{2\pi n}\, n^n\, e^{-n} \tag{53}$$

we can get the following close approximation at large k and high SNR:

$$\begin{aligned} C_{\text{QAM}}^{2k} &\lesssim \frac{1}{T}\log\left[\frac{2^k\pi^k\sqrt{2\pi k}k^k e^{-k}}{\sqrt{2\pi 2k}(2k)^{2k}e^{-2k}}\left(RHP\sqrt{\frac{T}{2}}\right)^{2k}\right] \\ &\quad - \frac{k}{T}\log\left(2\pi e\,\frac{N_0}{4}\right) \\ &= \frac{k}{T}\log\frac{(RHP)^2T}{2\cdot 2^{\frac{1}{2k}}kN_0}. \end{aligned} \tag{54}$$

Furthermore, substituting the system bandwidth of the multiple-subcarrier signal given by (6), we can get

$$C_{\mathrm{QAM}}^{2k} \lesssim \frac{k}{k+1} W \log \frac{(RHP)^2}{WN_0} \left(\frac{k+1}{k} \frac{1}{2 \cdot 2^{\frac{1}{2k}}} \right). \tag{55}$$

As the number of subcarriers k goes to infinity, the channel capacity converges to

$$\lim_{k \to \infty} C_{\mathrm{QAM}}^{2k} = W \log \left[\frac{(RHP)^2}{WN_0} \cdot \frac{1}{2} \right]. \tag{56}$$

Clearly, $(RHP)^2/WN_0 = \mathrm{SNR}/(k+1)$, and we can consider this quantity to be the SNR over the entire bandwidth occupied by the multiple-subcarrier signal. It must be greater than 2 to have reliable and nonclipping communications.

VII. Conclusion

In this correspondence, we have shown that, for multiple-subcarrier-modulated optical IM/DD channels, the input vectors must form finite p.s.d. sequences. These sequences are constrained inside the trigonometric moment spaces, which are convex hulls of certain space curves. We calculated the volume of the moment spaces and used it to find the upper bounds to the channel capacities for MSM systems with fixed bias.

Appendix
Proof of the Asymptotic Upper Bound

In this appendix, we prove that

$$h(\boldsymbol{Y}') \le h(\boldsymbol{X}_{\mathrm{unif}}) + o(\sigma) \tag{57}$$

where $o(\sigma) \to 0$ as $\sigma \to 0$.

To facilitate the proof, we first make and repeat a few definitions.

- Let
$$\mathcal{M}_k^P = \left\{ \boldsymbol{x} | \boldsymbol{x} = \frac{1}{T} \int_0^T x'(t)[v_n(t)]_{n=1}^k \, dt, \; x'(t) \ge 0, \; \frac{1}{T} \int_0^T x'(t) \, dt = 1 \right\}$$
be the k-dimensional cosine moment space.
- Let
$$z = \sqrt{-k\sigma^2 \log 2\pi\sigma^2 - \sigma^2 \log \sigma^2}$$
be the extension length.
- Let $d = \sup_{\boldsymbol{x} \in \mathcal{M}_k^P} \|\boldsymbol{x}\|$ be the longest convex hull radius.
- Let $R_1 = \{\boldsymbol{y} | \, \|\boldsymbol{y} - \boldsymbol{x}\| \le z, \text{ for any } \boldsymbol{x} \in \mathcal{M}_k^P\}$ be the extended convex hull.
- Let
$$R_2 = \{\boldsymbol{y} | \, \|\boldsymbol{y}\| \le d + z, \, \|\boldsymbol{y} - \boldsymbol{x}\| > z, \, \forall \boldsymbol{x} \in \mathcal{M}_k^P\}$$
be the gap region between the extended convex hull and the encircling hypersphere of origin 0 and radius $d + z$.
- Let $R_3 = \{\boldsymbol{y} | \boldsymbol{y} \notin R_1 \cup R_2\}$ be the region outside of the encircling hypersphere.

Also, the entropy of $\boldsymbol{Y}'$ is

$$\begin{aligned} h(\boldsymbol{Y}') &= \int_{y \in \mathbb{R}^k} -P_{\boldsymbol{Y}'} \log P_{\boldsymbol{Y}'} \, dy \\ &= \int_{y \in R_1} -P_{\boldsymbol{Y}'} \log P_{\boldsymbol{Y}'} \, dy \\ &\quad + \int_{y \in R_2} -P_{\boldsymbol{Y}'} \log P_{\boldsymbol{Y}'} \, dy \\ &\quad + \int_{y \in R_3} -P_{\boldsymbol{Y}'} \log P_{\boldsymbol{Y}'} \, dy. \end{aligned} \tag{58}$$

We define the following notation:

$$h_1(\boldsymbol{Y}') = \int_{y \in R_1} -P_{\boldsymbol{Y}'} \log P_{\boldsymbol{Y}'} \, dy \tag{59}$$

$$h_2(\boldsymbol{Y}') = \int_{y \in R_2} -P_{\boldsymbol{Y}'} \log P_{\boldsymbol{Y}'} \, dy \tag{60}$$

$$h_3(\boldsymbol{Y}') = \int_{y \in R_3} -P_{\boldsymbol{Y}'} \log P_{\boldsymbol{Y}'} \, dy. \tag{61}$$

A. Region I

First, we examine $h_1(\boldsymbol{Y}')$

$$\begin{aligned} h_1(\boldsymbol{Y}') &= \int_{y \in R_1} -P_{\boldsymbol{Y}'} \log P_{\boldsymbol{Y}'} \, dy \\ &= \int_{y \in R_1} -\left\{ \frac{P_{\boldsymbol{Y}'}}{P(y \in R_1)} P(y \in R_1) \right\} \\ &\quad \cdot \log \left\{ \frac{P_{\boldsymbol{Y}'}}{P(y \in R_1)} P(y \in R_1) \right\} dy \\ &= P(y \in R_1) \int_{y \in R_1} \\ &\quad - P_{\boldsymbol{Y}'|R_1} \left\{ \log P_{\boldsymbol{Y}'|R_1} + \log P(y \in R_1) \right\} dy \\ &= P(y \in R_1) h(\boldsymbol{Y}'|R_1) - P(y \in R_1) \log P(y \in R_1) \\ &\le P(y \in R_1) \left(h(\boldsymbol{X}_{\mathrm{unif}}) + k \log \left(1 + \frac{z}{d'} \right) \right) \\ &\quad - P(y \in R_1) \log P(y \in R_1) \\ &= (1 - P(y \in R_2 \cup R_3)) \\ &\quad \cdot \left(h(\boldsymbol{X}_{\mathrm{unif}}) + k \log \left(1 + \frac{z}{d'} \right) \right) \\ &\quad - P(y \in R_1) \log P(y \in R_1) \\ &= h(\boldsymbol{X}_{\mathrm{unif}}) + o_1(\sigma). \end{aligned} \tag{62}$$

Here $d' = \inf_{\boldsymbol{x} \in \mathcal{M}_k^P} \|\boldsymbol{x}\|$. What we are saying is that if we scale the original convex hull in all axes by a factor of $1 + z/d'$, we are obviously going to get a hull enclosing our extension R_1 and the volume of this scale extension is going to be $(1 + z/d')^k V_k^P$. We remark that, as $\sigma \to 0$, $P(y \in R_1) \to 1$ and $R_1 \to \mathcal{M}_k^P$. Therefore, $P(y \in R_2 \cup R_3) \to 0$, $P(y \in R_1) \log P(y \in R_1) \to 0$, and $z \to 0$. Thus, $h_1(\boldsymbol{Y}') \to h(\boldsymbol{X}_{\mathrm{unif}})$.

B. Probability Bound

Before we start to deal with regions II and III, we first make a claim about the probability density of $\boldsymbol{Y}'$ outside of region I.

The probability density of the k-dimensional Gaussian noise $\boldsymbol{N}'$ is

$$\begin{aligned} P_{\boldsymbol{N}'}(\boldsymbol{x}) &= \frac{1}{\sqrt{2\pi\sigma^2}^k} \exp \left(-\frac{\boldsymbol{x}^* I_k \sigma^2 \boldsymbol{x}}{2} \right) \\ &= \frac{1}{\sqrt{2\pi\sigma^2}^k} \exp \left(-\frac{\|\boldsymbol{x}\|^2}{2\sigma^2} \right) \\ &= \exp \left(-\frac{\|\boldsymbol{x}\|^2 + k\sigma^2 \log 2\pi\sigma^2}{2\sigma^2} \right). \end{aligned} \tag{63}$$

In a slight abuse of notation, we denote

$$P_{\boldsymbol{N}'}(\boldsymbol{x}) = P_{\|\boldsymbol{N}'\|}(\|\boldsymbol{x}\|). \tag{64}$$

Then, we have the probability density of $\boldsymbol{Y}'$ in regions II and III

$$P_{\boldsymbol{Y}'}(y) \le P_{\|\boldsymbol{N}'\|}(z), \qquad \text{for all } y \in R_2 \cup R_3 \tag{65}$$

where $P_{\|\boldsymbol{N}'\|}(\|\boldsymbol{x}\|)$ is defined as above and

$$z = \sqrt{-k\sigma^2 \log 2\pi\sigma^2 - \sigma^2 \log \sigma^2}.$$

We get this as follows:

$$\begin{aligned} P_{\boldsymbol{Y}'}(y) &= \int_{x \in \mathcal{M}_k^P} P_{\boldsymbol{N}'}(y-x) P_{\boldsymbol{X}}(x)\, dx \\ &= \int_{x \in \mathcal{M}_k^P} P_{\|\boldsymbol{N}'\|}(\|\boldsymbol{y}-\boldsymbol{x}\|) P_{\boldsymbol{X}}(x)\, dx \\ &\le \int_{x \in \mathcal{M}_k^P} P_{\|\boldsymbol{N}'\|}(z) P_{\boldsymbol{X}}(x)\, dx \\ &= P_{\|\boldsymbol{N}'\|}(z) = e^{\frac{\log \sigma^2}{2}} = \sigma. \end{aligned} \tag{66}$$

C. Region II

Then, we show that

$$\begin{aligned} h_2(\boldsymbol{Y}') &= \int_{y \in R_2} -P_{\boldsymbol{Y}'} \log P_{\boldsymbol{Y}'}\, dy \\ &\le -P_{\|\boldsymbol{N}'\|}(z) \log P_{\|\boldsymbol{N}'\|}(z) Vol(R_2). \end{aligned} \tag{67}$$

In showing this, we use the fact that $P_{\boldsymbol{Y}'}(y)$ disappears in region II when $\sigma \to 0$. Again, we remark that, as $\sigma \to 0$, $z \to 0$. Thus, the entropy $-P_{\|\boldsymbol{N}'\|}(z) \log P_{\|\boldsymbol{N}'\|}(z) \to 0$. The volume of R_2 is finite. Hence, $h_2(\boldsymbol{Y}') \to 0$.

D. Region III

At last, we show that the entropy in region III $h_3(\boldsymbol{Y})$ is bounded and diminishes asymptotically with σ^2. To show this, we need to change from Cartesian coordinates to polar coordinates and do a radial integration

$$\begin{aligned} h_3(\boldsymbol{Y}) &= \int_{y \in R_3} -P_{\boldsymbol{Y}} \log P_{\boldsymbol{Y}}\, dy \\ &\le \int_0^\infty -\left\{P_{\|\boldsymbol{N}\|}(z+r)\right\} \left\{\log P_{\|\boldsymbol{N}\|}(z+r)\right\} \\ &\quad \cdot \left\{\text{surface}(d+z+r)\right\} dr \\ &= \int_z^\infty -P_{\|\boldsymbol{N}\|}(r) \log P_{\|\boldsymbol{N}\|}(r\{\text{surface}(d+r)\}\, dr. \end{aligned} \tag{68}$$

Here, the function $\text{surface}(d+r)$ is the surface area of the k-dimensional encircling sphere with radius $d+r$. We know that

$$\text{surface}_k\{d+r\} = k\pi^{\frac{k}{2}}(d+r)^{k-1}/\Gamma\left(\frac{k}{2}+1\right)$$

and $d = \sqrt{k}$. Define $S_k = k\pi^{\frac{k}{2}}/\Gamma(\frac{k}{2}+1)$. Then

$$\begin{aligned} h_3(\boldsymbol{Y}) &\le S_k \int_z^\infty -P_{\|\boldsymbol{N}\|}(r) \log P_{\|\boldsymbol{N}\|}(r)(d+r)^{k-1}\, dr \\ &= -S_k \int_z^\infty \frac{1}{\sqrt{2\pi\sigma^2}^k} e^{-\frac{r^2}{2\sigma^2}} \\ &\quad \cdot \left\{-\frac{r^2}{2\sigma^2} - k \log \sqrt{2\pi\sigma^2}\right\} (d+r)^{k-1}\, dr. \end{aligned} \tag{69}$$

We now change a variable. Let $x = \frac{r}{\sigma}$. Then

$$\begin{aligned} h_3(\boldsymbol{Y}) \le -S_k \int_{\frac{z}{\sigma}}^\infty & \frac{1}{\sqrt{2\pi\sigma^2}^k} e^{-\frac{x^2}{2}} \\ & \cdot \left\{-\frac{x^2}{2} - k \log \sqrt{2\pi\sigma^2}\right\} (d+\sigma x)^{k-1} \sigma\, dx. \end{aligned} \tag{70}$$

We claim that when σ approaches 0, the right-hand side approaches 0. Without loss of generality, we assume that $\sigma \le 1$. This assumption is equivalent to requiring the noise power to be less than the signal power

$$\begin{aligned} h_3(\boldsymbol{Y}) \le & -S_k \int_{\frac{z}{\sigma}}^\infty \frac{1}{\sqrt{2\pi\sigma^2}^k} e^{-\frac{x^2}{2}} \\ & \cdot \left\{-\frac{x^2}{2} - k \log \sqrt{2\pi\sigma^2}\right\} (d+\sigma x)^{k-1} \sigma\, dx \\ = & S_k \int_{\frac{z}{\sigma}}^\infty \frac{1}{\sqrt{2\pi\sigma^2}^k} e^{-\frac{x^2}{2}} \frac{x^2}{2} (d+\sigma x)^{k-1} \sigma\, dx \\ & + S_k k \log \sqrt{2\pi\sigma^2} \int_{\frac{z}{\sigma}}^\infty \frac{1}{\sqrt{2\pi}} e^{-\frac{x^2}{2}} (d+\sigma x)^{k-1} \sigma\, dx. \end{aligned} \tag{71}$$

If σ is small enough (i.e., $\frac{z}{\sigma}$ is big), then we know that there exists $\delta > 0$ such that

$$e^{-\frac{x^2}{2(1+\delta)}} \ge e^{-\frac{x^2}{2}} \frac{x^2}{2} (d+\sigma x)^{k-1}, \qquad \forall x \ge \frac{z}{\sigma}. \tag{72}$$

Therefore,

$$\begin{aligned} h_3(\boldsymbol{Y}) \le & \frac{S_k\sqrt{1+\delta}}{\sqrt{2\pi\sigma^2}^{k-1}} \int_{\frac{z}{\sigma}}^\infty \frac{1}{\sqrt{2\pi(1+\delta)}} e^{-\frac{x^2}{2(1+\delta)}}\, dx \\ & + \frac{S_k\sqrt{1+\delta}\log\sqrt{2\pi\sigma^2}}{\sqrt{2\pi\sigma^2}^{k-1}} \\ & \cdot \int_{\frac{z}{\sigma}}^\infty \frac{1}{\sqrt{2\pi(1+\delta)}} e^{-\frac{x^2}{2(1+\delta)}}\, dx \\ = & \frac{S_k\sqrt{1+\delta}}{\sqrt{2\pi\sigma^2}^{k-1}} Q\left(\frac{z}{\sigma\sqrt{1+\delta}}\right) \\ & + \frac{S_k\sqrt{1+\delta}\log\sqrt{2\pi\sigma^2}}{\sqrt{2\pi\sigma^2}^{k-1}} Q\left(\frac{z}{\sigma\sqrt{1+\delta}}\right). \end{aligned} \tag{73}$$

Thus, as $\sigma \to 0$, $h_3(\boldsymbol{Y}) \to 0$.

E. Conclusion

We now sum up the results for the three regions

$$\begin{aligned} \sup_{P_{\boldsymbol{X}}} h(\boldsymbol{Y},\sigma) &\le \sup_{P_{\boldsymbol{X}}} h_1(\boldsymbol{Y},\sigma) + h_2(\boldsymbol{Y},\sigma) + h_3(\boldsymbol{Y},\sigma) \\ &\le \sup_{P_{\boldsymbol{X}}} h_1(\boldsymbol{Y},\sigma) + \sup_{P_{\boldsymbol{X}}} h_1(\boldsymbol{Y},\sigma) + \sup_{P_{\boldsymbol{X}}} h_1(\boldsymbol{Y},\sigma). \end{aligned} \tag{74}$$

Then

$$\begin{aligned} \lim_{\sigma\to 0} \sup_{P_{\boldsymbol{X}}} h(\boldsymbol{Y},\sigma) &\le \lim_{\sigma\to 0} \left(\sup_{P_{\boldsymbol{X}}} h_1(\boldsymbol{Y},\sigma) + \sup_{P_{\boldsymbol{X}}} h_1(\boldsymbol{Y},\sigma) \right. \\ &\qquad \left. + \sup_{P_{\boldsymbol{X}}} h_1(\boldsymbol{Y},\sigma)\right) \\ &= h(\boldsymbol{X}_{\text{unif}}). \end{aligned} \tag{75}$$

Thus, the claim is proven.

ACKNOWLEDGMENT

The authors wish to thank Prof. D. Tse and L. Zheng for many helpful discussions. They also thank the anonymous reviewers for many constructive suggestions.

REFERENCES

[1] J. A. C. Bingham, "Multicarrier modulation for data transmission: An idea whose time has come," *IEEE Commun. Mag.*, vol. 28, pp. 5–14, May 1990.

[2] J. M. Kahn and J. R. Barry, "Wireless infrared communications," *Proc. IEEE*, vol. 85, pp. 265–298, Feb. 1997.

[3] J. B. Carruthers and J. M. Kahn, "Modeling of nondirected wireless infrared channels," *IEEE Trans. Commun.*, vol. 45, pp. 1260–1268, Oct. 1997.

[4] K. Fan, "On positive definite sequences," *Ann. Math.*, vol. 47, no. 3, pp. 593–607, July 1946.

[5] R. You and J. M. Kahn, "Average power reduction techniques for multiple-subcarrier intensity-modulated optical signals," *IEEE Trans. Commun.*, to be published.

[6] U. Grenander and G. Szego, *Toeplitz Forms and Their Applications*. Berkeley, CA: Univ. Calif. Press, 1958, pp. 16–19.

[7] J. Makhoul, "Toeplitz determinants and positive semidefiniteness," *IEEE Trans. Signal Processing*, vol. 39, pp. 743–746, Mar. 1991.

[8] R. T. Rockafellar, *Convex Analysis*. Princeton, NJ: Princeton Univ. Press, 1970.

[9] I. J. Schoenberg, "An isoperimetric inequality for closed curves convex in even-dimensional Euclidean spaces," *Acta Math.*, vol. 91, pp. 143–164, Oct. 1954.

[10] J. Makhoul, "Volume of the space of positive definite sequences," *IEEE Trans. Acoust., Speech, Signal Processing*, vol. 38, pp. 506–511, Mar. 1990.

[11] S. Karlin and W. J. Studden, *Tchebycheff Systems: With Applications in Analysis and Statistics*. New York: Interscience, 1966, pp. 127–129.

The Index Entropy of a Mismatched Codebook

Ram Zamir, *Senior Member, IEEE*

***Abstract*—Entropy coding is a well-known technique to reduce the rate of a quantizer. It plays a particularly important role in universal quantization, where the quantizer codebook is not matched to the source statistics. We investigate the gain due to entropy coding by considering the entropy of the index of the first codeword, in a mismatched random codebook, that D-matches the source word. We show that the index entropy is strictly lower than the "uncoded" rate of the code, provided that the entropy is conditioned on the codebook. The number of bits saved by conditional entropy coding is equal to the divergence between the "favorite type" (the limiting empirical distribution of the first D-matching codeword) and the codebook-generating distribution. Specific examples are provided.**

***Index Terms*—Entropy-coded quantization, favorite type, mismatched source coding, universal quantization.**

I. INTRODUCTION

Entropy coding is an efficient method for enhancing quantizer performance [6], [2]. This correspondence investigates the role of entropy coding when the quantizer codebook is *mismatched* with respect to the source distribution.

Manuscript received April 29, 2001; revised August 27, 2001. This work was supported in part by the United States–Israel Binational Science Foundation under Grant 1998-309. The material in this correspondence was presented in part at the International Symposium on Information Theory, Sorrento, Italy, June 2000.

The author is with the Department of Electrical Engineering–Systems, Tel-Aviv University, Tel-Aviv 69978, Israel (e-mail: zamir@eng.tau.ac.il).

Communicated by P. A. Chou, Associate Editor for Source Coding.

Publisher Item Identifier S 0018-9448(02)00317-6.

The setting of optimum entropy coding of a mismatched codebook is typical of universal quantization [16]. Although our main motivation originates from structured (e.g., lattice) codes and real-valued processes, we confine our discussion to random codes and to discrete memoryless sources. Our results are based on recent work by Yang and Kieffer [11] and by Zamir and Rose [13] in the area of mismatched codes.

Specifically, we investigate the entropy rate of the index of the first codeword in $\{\boldsymbol{Y}_1, \boldsymbol{Y}_2, \ldots\}$ which satisfies $d(\boldsymbol{X}, \boldsymbol{Y}_n) \leq D$ ("D-match"), where $\boldsymbol{X}$ is a source l-word generated independent and identically distributed (i.i.d) $\sim P$, and $\{\boldsymbol{Y}_1, \boldsymbol{Y}_2, \ldots\}$, the codebook, is an infinite list of random code l-words drawn i.i.d. $\sim Q$. Let N_l denote the index n of the first D-matching codeword. Our main result characterizes the entropy rate of N_l in terms of single-letter information quantities. It implies, for example, that the difference between the index entropy and the conditional index entropy (conditional on the codebook) is given by

$$\lim_{l\to\infty} \frac{1}{l} H(N_l) - \lim_{l\to\infty} \frac{1}{l} H(N_l|\boldsymbol{Y}_1, \boldsymbol{Y}_2, \ldots) = D(Q^*_{P,Q,D}\|Q)$$

where $D(\cdot)$ denotes divergence, and the distribution $Q^*_{P,Q,D}$, called the "favorite type," is the limiting empirical distribution of the first D-matching codeword [13].

Section II defines the setting, introduces some useful information quantities, and gives the main result. Section III illustrates this result by an explicit example, and Section IV gives the proof. In a future work with Kontoyiannis [8], we will extend these concepts to general alphabets and source distributions, and demonstrate their tight relation to dithered lattice (universal) quantization [16], [12].

II. PRELIMINARIES AND MAIN RESULT

Consider coding a source string $\boldsymbol{X} = X_1 \cdots X_l$ from a finite alphabet $\mathcal{X}$ into a codeword $\boldsymbol{y} = y_1 \cdots y_l$ from a finite alphabet $\mathcal{Y}$ under the distortion constraint

$$d(\boldsymbol{X}, \boldsymbol{y}) \triangleq 1/l \sum_{i=1}^{l} d(X_i, y_i) \leq D \tag{1}$$

where $d\colon \mathcal{X} \times \mathcal{Y} \to [0, \infty)$ is a finite distortion measure. If (1) holds, we say that "$\boldsymbol{y}$ D-matches $\boldsymbol{X}$." We shall assume that $\boldsymbol{X}$ is generated by a memoryless source having a distribution $P = \{P(x), x \in \mathcal{X}\}$.

Suppose a random codebook $\boldsymbol{Y}_1, \boldsymbol{Y}_2, \ldots$ of words in $\mathcal{Y}^l$ is generated such that each letter in each codeword is i.i.d. as $Q = \{Q(y), y \in \mathcal{Y}\}$. Let N_ℓ denote the index of the first codeword that satisfies (1), i.e.,

$$d(\boldsymbol{X}, \boldsymbol{Y}_i) > D, \qquad i = 1, \ldots, N_l - 1,\ d(\boldsymbol{X}, \boldsymbol{Y}_{N_l}) \leq D.$$

To avoid technical subtleties we assume that the distortion measure is such that every source letter has a perfect reconstruction letter, i.e., for each x

$$d(x, y) = 0, \qquad \text{for some } y. \tag{2}$$

We also assume that $Q(y) > 0$ for all y in $\mathcal{Y}$. It follows that for any source string $\boldsymbol{x}$ and $D \geq 0$, there is a positive probability $p_{\text{match}} > 0$ that each codeword $\boldsymbol{Y}_i$ will D-match $\boldsymbol{x}$. As a consequence

$$\Pr\{N_l < \infty \,|\, \boldsymbol{X} = \boldsymbol{x}\} = 1$$

i.e., a D-match is found in the codebook with probability one. See, e.g., [10], [15], [9], [11], [5] and the references therein, for various settings of lossy source coding and the related topic of approximate string matching.